AIAA 2001-0931

MODELLING THE RESTRAINT OF LIQUID JETS BY SURFACE TENSION IN MICROGRAVITY

David J. Chato and David A. Jacqmim
NASA Glenn Research Center
Cleveland, Ohio

39th AIAA Aerospace Sciences Meeting & Exhibit
8-11 January 2001 / Reno, NV

MODELLING THE RESTRAINT OF LIQUID JETS BY SURFACE TENSION IN MICROGRAVITY
By
David J. Chato and David A. Jacqmin
NASA Glenn Research Center

Abstract

An axisymetric phase field model is developed and used to model surface tension forces on liquid jets in microgravity. The previous work in this area is reviewed and a baseline drop tower experiment selected for model comparison. A mathematical model is developed which includes a free surface. a symmetric centerline and wall boundaries with given contact angles. The model is solved numerically with a compact fourth order stencil on a equally spaced axisymmetric grid. After grid convergence studies, a grid is selected and all drop tower tests modeled. Agreement was assessed by comparing predicted and measured free surface rise. Trend wise agreement is good but agreement in magnitude is only fair. Suspected sources of disagreement are suspected to be lack of a turbulence model and the existence of slosh baffles in the experiment which were not included in the model.

Nomenclature

We = Weber Number
ρ = density
u = velocity
r = jet radius
σ = surface tension
f = free energy
α = constant 1
β = constant 2
C = phase distrubution
ψ = barrier function
V = volume
ϕ = potention function
P = pressure
x = distance
g = wall function
M = radial correction factor
θ_c = contact angle
a = height
d = jet diameter
D = tank dimater
L = tank length
Re = Renolds Number

Introduction

Microgravity poses many challenges to the designer of spacecraft tanks. Chief among these are the lack of phase separation in the fluid and the need to supply vapor-free liquid or liquid free vapor to the required spacecraft processes. One of the principal problems of phase separation is the creation of liquid jets. A jet can be created by liquid filling, settling of the fluid to one end of the tank, or even closing a valve to stop the liquid outflow. In normal gravity the gravitational force controls and restricts the liquid jet flow, but in microgravity with gravity largely absent, jets must be contained by surface tension forces. Recent NASA experiments in microgravity (TPCE and VTRE) have brought a wealth of data of jet behavior in microgravity. VTRE was surprising in that although it contained a complex geometry of baffles and vanes the limit on liquid inflow was the emergence of a liquid jet from the top of the vane structure. Clearly understanding the restraint of liquid jets by surface tension is key to managing fluids in low gravity.

Flow of a submerged axial jet constrained by surface tension is similar to stagnation flow against a plate in that the jet hits the constraining surface and is deflected radially out. However, the ability of the constraining surface to move in response to the exerted force is unique. In fact to increase the restraining force on the jet as flow rate increases, the surface must deform to increase the radius of curvature of the free surface, thereby increasing the surface tension force. Unfortunately this motion also changes the direction in which the surface tension force acts. Eventually the limit is reached where the surface tension force is perpendicular to flow and hence no longer retains it. When the deformation of the free surface is large the restraining bulge is long and slender. At this point several other mechanisms act to break down the jet, such as columnar buckling or the Taylor Instability where surface waves grow to such amplitude that they pinch a droplet off from the jet.

To model this phenomenon a numerical method that tracks the fluid motion and the surface tension forces is required. Jacqmin[1] has developed a phase-field model that converts the delta-function surface tension force into a continuum function that peaks at the free surface and decays rapidly away. Previous attempts at this formulation have been criticized for smearing the interface but by sharpening the phase function, double gridding the fluid function and using a higher order solution for the fluid function these concerns have been ameliorated.

Review of Literature

NASA Drop Tower Data is found in references 2-13. Symons[2-5] and Spuckler[7] studied the liquid inflow via axial jet into a broad range of tank shapes both empty and partially full. Symons work establishes an empirical limit for jets of Weber number (We) equal to 1.3-1.5 depending on jet velocity profile, where:

$$We = \frac{\rho u_{av}^2 r}{2\sigma} \tag{1}$$

$\rho = density$
$u_{av} = average\ jet\ velocity$
$r = jet\ radius$
$\sigma = surface\ tension$

Staskus[6] extends the work of Symons by placing baffles in front of the jet. However, no attempt is made to analyze these complex flows. Instead results are reported as a ratio of improvement to the unbaffled jet Weber number. Labus[8] also studies the effect of baffles including ones that break the central jet into several small jets. Aydelott[10, 12-13] looks at the problem of a recirculating jet where the liquid level is held constant. Results are classified into four flow patterns, dissipation, geyser formation, aft collection, and circulation. It is the geyser formation/aft collection we concern ourselves with in this paper. Aydelott's assessment that a drop in mixing accompanies this transition indicates the transition's importance. Labus[11] studies both stagnation flow and free surface shape, but is concerned with the back of a flow stagnated against a flat plate in microgravity.

Shuttle based experiments in references 14-18 provide valuable flight data. Video of Plexiglas tanks during shuttle flight provide several improvements over drop tower tests; including increasing the scale from 4" tanks to 12" tanks and extending the duration of test from 5 seconds to half-an-hour. Tank Pressure Control

Experiment is the first of these and has flown three times. The first flight focused on the mixing studies of Aydelott. Improvements included actual heat transfer data by using a condensing fluid (refrigerant 113) and longer duration. Bentz[14-16] was able to confirm the geysering and circulating regimes of Aydelott, but encountered an asymmetric regime between the two that was even more catastrophic to heat transfer than aft collection. The second flight of TPCE focused mostly on rapid boiling phenomena, but contains some further tests on mixing. Hasan[17] confirms the findings of Bentz. The third flight[18] was done at a lower fill level but confirms the results of the other flights. The Vented Tank Resupply Experiment[19] was designed to look at vanes rather than axial jets, but as noted previously exhibits the classic gesyering behavior.

Analytical work is listed in references 20-30. Concus[20-21] provides differential equations of the free surface problem, but analyzes only static cases. Nickell[22] analyzes flow from a jet into a liquid and the resultant free surface shape for a normal gravity application, but removes all surface tension from the analysis as secondary. Hochstein[23-24] analyzes the microgravity mixing with a volume of fluid approach, but uses only a limited approximation to model the surface tension. Aydelott[25] and Der[26] both analyze the motion of a bubble in the oxygen tank during separation of a Centaur stage with VOF models; noteworthy in these is again the appearance of a geyser. Tegart[27] shows the application of the surface Evolver code of Brakke[28] to actual tank shapes. Brackbill[29] develops an improved surface tension model for VOF codes, but only shows one example of its use for axial jets. Shrader[30] uses a Runga-Kutta scheme to solve the differential equation of free surface deformation in response to an imposed pressure field. This approach is quite promising but does not always converge and limits the interaction between the flow field and the free surface. Jacqmin[1] developed a phase field model of surface tension and implemented as a fourth order accurate scheme using a compact 9-point stencil. Although Jacqmin lays out the basic axisymmetric scheme the computer code and all the examples in his paper are planar. The Jacqmin model will serve as the basis for the present analysis

Model

Introduction

To model the fluid motion the Navier-Stokes equations are formulated for low-speed incompressible flow. Velocity and pressure are placed on a staggered grid,

with velocity being tracked at cell faces and pressure at cell centers. To track the free surface a color function is introduced which tracks liquid as 1/2 and gas as -1/2. Jacqmin has developed a phase-field model that converts the delta-function surface tension force into a continuum function that peaks at the free surface and decays rapidly away. Previous attempts at this formulation have been criticized for smearing the interface but by sharpening the phase function, double gridding the fluid function and using a higher order solution for the fluid function these concerns have been ameliorated. This paper will document the adaptation of the Jacqmin algorithm to the problem of restraint of liquid jets. The enhancements include formulation of an axisymmetric fourth order model, implementation of a symmetric boundary condition at the tank centerline, and extension of the wall wetting boundary condition to fourth order accuracy. A simple velocity forcing function has been added to simulate the jet without violating continuity.

Phase Model of Surface Tension

Surface tension can be expressed as a free energy field. The expression for this energy in our formulation is given by

$$f = \tfrac{1}{2}\alpha |\nabla C|^2 + \beta \Psi(C) \qquad (2)$$

Where C is a phase distribution function and ψ is a barrier function that is maximum at the interface and dies away as the phase becomes uniform. This formulation is extracted from Van der Waals[31] and inherently implies that the equilibrium free surface position is the one where the free energy is minimized. In order to model this behavior the physical ψ that dies away on the molecular scale is approximated by a function with similar behavior on a larger scale such as

$$\Psi(C) = \frac{2^{2k}}{2k+2} C^{2k+2} - \frac{1}{2} C^2 + \frac{2k}{8(2k+2)} \qquad (3)$$

This function has the required properties of being maximum at C=0 and dying away to 0 at both 1/2 and -1/2. If we define our C function as being 1/2 when the phase is liquid and -1/2 when the phase is gas this will produce the required behavior. Higher values of k produce sharper peaks. For our solution we will choose k = 16.

To study the transients of the free surface some additional formulations are required. We define a potential function as the rate of change in f per unit volume with respect to C.

$$\phi = \frac{\delta \int f dV}{\delta C} = \beta \Psi'(C) - \alpha \nabla^2 C \qquad (4)$$

Cahn and Hilliard[32] approximate the transients of the free surface by setting the diffusion fluxes as proportional to the potential gradient. In equation form this is

$$\frac{\partial C}{\partial t} = \kappa \nabla^2 \phi \qquad (5)$$

This gives us two coupled Possion equations to solve for the phase distribution. To add the effects of fluid motion we must use the Navier-Stokes equations. The continuity equation for incompressible flow is

$$\vec{\nabla} \bullet \vec{u} = 0 \qquad (6)$$

The momentum equations for each direction are given by

$$\rho \frac{Du_i}{Dt} = \rho \frac{\partial u_i}{\partial t} + \rho \sum_j u_j \frac{\partial u_i}{\partial x_j} =$$
$$-\vec{\nabla}P + \mu \nabla^2 u_i - C\vec{\nabla}\phi \qquad (7)$$

Fourth Order Formulation of the Governing Equations

The equations of the previous section cannot be solved directly but must be solved numerically. To keep the interface as sharp as possible a compact 4th order stencil is used

The mehrstellungen method

The equation

$$\nabla^2 u = f \qquad (8)$$

Was show by Collatz[33] to be approximated by

$$\left[\nabla^2 + \frac{1}{12}(\Delta x)^2 \nabla^4 \right] u = f + \frac{1}{12} \nabla^2 f$$
$$+ O(\Delta x^4) \qquad (9)$$

Using central differencing on a square Cartesian grid one obtains the following computational stencil

$$\frac{1}{6}\begin{bmatrix} 1 & 4 & 1 \\ 4 & -20 & 4 \\ 1 & 4 & 1 \end{bmatrix} u = \frac{(\Delta x)^2}{12}\begin{bmatrix} 0 & 1 & 0 \\ 1 & 8 & 1 \\ 0 & 1 & 0 \end{bmatrix} f \qquad (10)$$
$$+ O(\Delta x^4)$$

3

.With some slight modification we can use this to rewrite the potential equation as

$$\frac{\alpha}{6(\Delta x)^2}\begin{bmatrix} 1 & 4 & 1 \\ 4 & -20 & 4 \\ 1 & 4 & 1 \end{bmatrix}C =$$

$$\frac{\beta}{12}\begin{bmatrix} 0 & 1 & 0 \\ 1 & 8 & 1 \\ 0 & 1 & 0 \end{bmatrix}\Psi'(C) - \begin{bmatrix} 0 & 0 & 0 \\ 0 & 1 & 0 \\ 0 & 0 & 0 \end{bmatrix}\phi \qquad (11)$$

$$+\frac{(\Delta x)^2}{12}\nabla^2\phi + O(\Delta x^4)$$

We retain the $\nabla^2\phi$ term because it can be calculated by equation 5.

Application to an Axisymmetric Grid

In axisymmetric coordinates our equation becomes

$$\frac{\alpha}{6(\Delta x)^2}\begin{bmatrix} M_- & 4 & M_+ \\ 4M_- & -20 & 4M_+ \\ M_- & 4 & M_+ \end{bmatrix}C =$$

$$\frac{\beta}{12}\begin{bmatrix} 0 & 1 & 0 \\ M_- & 8 & M_+ \\ 0 & 1 & 0 \end{bmatrix}\Psi'(C) \qquad (12)$$

$$-\begin{bmatrix} 0 & 0 & 0 \\ 0 & 1 & 0 \\ 0 & 0 & 0 \end{bmatrix}\phi + \frac{(\Delta r)^2}{12}\nabla^2\phi + O(\Delta r^4)$$

where

$$M_\pm = (r_\pm + r_0)/2r_0 \qquad (13)$$

Symmetry Boundary

At the center line (r=0) the problem is symmetric Therefore along this edge the equation becomes:

$$\frac{\alpha}{6(\Delta x)^2}\begin{bmatrix} 2 & 4 \\ -28 & 16 \\ 2 & 4 \end{bmatrix}C = \frac{\beta}{12}\begin{bmatrix} 1 & 0 \\ 6 & 4 \\ 1 & 0 \end{bmatrix}\Psi'(C)$$

$$\qquad (14)$$

$$-\begin{bmatrix} 0 & 0 \\ 1 & 0 \\ 0 & 0 \end{bmatrix}\phi + \frac{(\Delta r)^2}{12}\nabla^2\phi + O(\Delta r^4)$$

Wall Boundaries

At the outer wall two boundary conditions will be used. First is the no flux boundary

$$\frac{\partial\phi}{\partial r} = 0 \qquad (15)$$

The second is a bit more complicated. Postulating a wall energy function of the form

$$f_w = \int\sigma g(C)dA \qquad (16)$$

where g is a function chosen to yield the correct contact angle, then the diffusively controlled equilibrium at the wall is

$$\alpha\frac{\partial C}{\partial r} + \sigma g'(C) = 0 \qquad (17)$$

for our purposes

$$g(C) = \cos(\theta_c)\left[6C^2 - 1.5\right] \qquad (18)$$

where θ_c is the static contact angle at the side wall. For the experiment modeled the contact angle is zero so $\cos(\theta_c)$ is one.

Substituting into our main equation

$$\frac{\alpha}{6(\Delta x)^2}\begin{bmatrix} 2 & 4 \\ 8-4\frac{\Delta r}{r} & -20+4\frac{\Delta r}{r} \\ 2 & 4 \end{bmatrix}C =$$

$$\frac{\beta}{12}\begin{bmatrix} 0 & 1 \\ 2 & 8 \\ 0 & 1 \end{bmatrix}\Psi'(C) - \begin{bmatrix} 0 & 0 \\ 1 & 0 \\ 0 & 0 \end{bmatrix}\phi \qquad (19)$$

$$+\frac{(\Delta r)^2}{12}\nabla^2\phi + (\frac{2}{\Delta r} + \frac{1}{3r} + \frac{\Delta r}{3r^2})g'$$

$$+(\frac{\Delta x}{6} - \frac{\Delta x^2}{12r})\Psi''\frac{\beta}{\alpha}g' + O(\Delta x^4)$$

A similar approach is used for the top wall except that for simplicity θ_c is set to 90° resulting in g=g'=0 and the boundary being symmetric. This should not affect the results of the calculation since interface flow along the top wall does not occur in our problem until after free surface penetration. The equation for the top wall is

$$\frac{\alpha}{6(\Delta r)^2}\begin{bmatrix} 4M_- & -20 & 4M_+ \\ 2M_- & 8 & 2M_+ \end{bmatrix} C =$$

$$\frac{\beta}{12}\begin{bmatrix} M_- & 8 & M_+ \\ 0 & 2 & 0 \end{bmatrix}\Psi'(C) - \begin{bmatrix} 0 & 1 & 0 \\ 0 & 0 & 0 \end{bmatrix}\phi \quad (20)$$

$$+\frac{(\Delta r)^2}{12}\nabla^2\phi + O(\Delta r^4)$$

The bottom wall is done the same as the top wall. Here the logic used to justify θ_c is set to 90° is that the wall is only in contact with liquid throughout our runs. The equation for the bottom wall is

$$\frac{\alpha}{6(\Delta r)^2}\begin{bmatrix} 2M_- & 8 & 2M_+ \\ 4M_- & -20 & 4M_+ \end{bmatrix} C =$$

$$\frac{\beta}{12}\begin{bmatrix} 0 & 2 & 0 \\ M_- & 8 & M_+ \end{bmatrix}\Psi'(C) - \begin{bmatrix} 0 & 0 & 0 \\ 0 & 1 & 0 \end{bmatrix}\phi \quad (21)$$

$$+\frac{(\Delta r)^2}{12}\nabla^2\phi + O(\Delta r^4)$$

Corner Boundaries

Equation for the top inner boundary combining the symmetry and top wall boundaries

$$\frac{\alpha}{6(\Delta r)^2}\begin{bmatrix} -28 & 16 \\ 4 & 8 \end{bmatrix} C = \frac{\beta}{12}\begin{bmatrix} 6 & 4 \\ 2 & 0 \end{bmatrix}\Psi'(C)$$

$$-\begin{bmatrix} 1 & 0 \\ 0 & 0 \end{bmatrix}\phi + \frac{(\Delta r)^2}{12}\nabla^2\phi + O(\Delta r^4) \quad (22)$$

Equation for the bottom inner boundary combing symmetry and bottom wall boundary

$$\frac{\alpha}{6(\Delta r)^2}\begin{bmatrix} 4 & 8 \\ -28 & 16 \end{bmatrix} C = \frac{\beta}{12}\begin{bmatrix} 2 & 0 \\ 6 & 4 \end{bmatrix}\Psi'(C)$$

$$-\begin{bmatrix} 0 & 0 \\ 1 & 0 \end{bmatrix}\phi + \frac{(\Delta r)^2}{12}\nabla^2\phi + O(\Delta r^4) \quad (23)$$

Equation for the top outer boundary combining top and outer boundary

$$\frac{\alpha}{6(\Delta r)^2}\begin{bmatrix} 8-4\dfrac{\Delta r}{r} & -20+4\dfrac{\Delta r}{r} \\ 4 & 8 \end{bmatrix} C =$$

$$\frac{\beta}{12}\begin{bmatrix} 2 & 8 \\ 0 & 2 \end{bmatrix}\Psi'(C) - \begin{bmatrix} 0 & 1 \\ 0 & 0 \end{bmatrix}\phi \quad (24)$$

$$+\frac{(\Delta r)^2}{12}\nabla^2\phi + \left(\frac{2}{\Delta r}+\frac{1}{3r}+\frac{\Delta r}{3r^2}\right)g'$$

$$+\left(\frac{\Delta r}{6}-\frac{\Delta r^2}{12r}\right)\Psi''\frac{\beta}{\alpha}g' + O(\Delta x^4)$$

Equation for the bottom outer boundary

$$\frac{\alpha}{6(\Delta r)^2}\begin{bmatrix} 4 & 8 \\ 8-4\dfrac{\Delta r}{r} & -20+4\dfrac{\Delta r}{r} \end{bmatrix} C =$$

$$\frac{\beta}{12}\begin{bmatrix} 0 & 2 \\ 2 & 8 \end{bmatrix}\Psi'(C) - \begin{bmatrix} 0 & 0 \\ 0 & 1 \end{bmatrix}\phi \quad (25)$$

$$+\frac{(\Delta r)^2}{12}\nabla^2\phi + \left(\frac{2}{\Delta r}+\frac{1}{3r}+\frac{\Delta r}{3r^2}\right)g'$$

$$+\left(\frac{\Delta r}{6}-\frac{\Delta r^2}{12r}\right)\Psi''\frac{\beta}{\alpha}g' + O(\Delta r^4)$$

Implementation as a CFD code

The previous equations form a complete set of differential equations that can be solved for the fluid transient motion. Each equation is solved sequentially and numeric techniques specific to each equation are used to achieve the desired level of accuracy.

Solution for the potential field

A Newton-Rhapson iteration is used to project the body centered values of C to the cell boundaries and produce a ϕ field consistent with equation (5)

Advection of phase quantities

The equation (12) and its boundary equations form a matrix equation that is solved using the current values of C and ϕ to project new values. This process is iterated four times to smooth the solution.

Solution of the velocity field

Equation (7) is used to predict the change in velocity field. The projected velocity changes are used to calculate viscous stresses that are then used to correct the velocity change.

5

Solution of the pressure equation

The velocity changes are fed into the pressure Poisson equation that is solved by successive over relaxation to produce a uniform static pressure field consistent with our incompressible flow assumption.

Approximation of the Liquid Jet

Since the solution of the Navier-Stokes equation we used conserves mass strongly creating source and sink flows pose many difficulties. To avoid these problems the entering jet was modeled as a recirculating region where the v velocity was forced to a desired value. This allowed the u velocity to entrain liquid into the jet and thus conserve mass. A 0.5 cm length for this region was chosen since this appeared to be long enough so at the top of the region the mass entrainment was sufficient such that the v velocity was the dominant fluid motion.

Comparison to Experiment

Model Runs of Test Cases

After implementation of the code in axisymmetric form was complete and verified by several test cases, the drop tower runs of Aydelott were modeled. Aydelott looked at the problem of a recirculating jet where the liquid level is held constant. Results are classified into four flow patterns, dissipation, geyser formation, aft collection, and circulation. It is the dissipation/geyser formation we concern ourselves with in this paper. Table 1 shows a compilation of Aydelott's zero-g runs in these regimes. Little of the drop tower film remains, but figure 1 shows the time history of run 15 (Re 450, Fill level 50%). Times are estimated from frame counts since the clock is out of focus. Spherical tank data has been omitted since we cannot model curved boundaries. Aydelott's assessment that this transition is accompanied by a drop in mixing indicates the transition's importance. As a turbulence model for this formulation is not yet available the work of Aydelott was deemed the most suitable since it contains a number of cases observed by the author to be either laminar or transitional with Reynolds number between 450 and 1290. Figures 2-4 show representative computer predictions of these tests. Figure 2 is a low flow rate test that only slightly deforms the free surface. Figure 3 is a medium flow rate test that forms a geyser in the center but reaches a steady flow condition. Figure 4 is a high flow rate test where the geyser continues to grow throughout until it eventually contacts the far boundary of the grid. The model handed the free

Table 1 Experimental Results of Aydelott

Test	Tank Shape	Liquid Fill Vol %	Jet Reynolds no	Jet Weber no	Ratio of Geyser height to tank Diameter
1	c	29	630	0.96	0.55
2	c	29	900	1.09	.80
12	b	39	450	.49	.36
13	b	39	900	1.11	.84
14	b	39	1290	1.59	2.16
15	c	50	450	.39	.42
17	c	51	630	.78	.34
19	c	52	900	.81	.52
24	a	52	1320	1.16	1.45
50	b	60	450	.37	.24
51	b	60	900	.72	.42
52	b	60	1320	1.05	1.10
53	b	73	900	.57	.30
57	b	73	1270	.78	.70
64	b	91	480	.31	.10
65	c	91	900	.48	.20
66	c	92	1290	.62	.48

surface deformation quite nicely, even to the point of modeling geyser growth in the regime where the free surface is no longer restrained.

<u>Grid sensitivity</u>

A grid sensitivity test was done to confirm the choice of a 50 by 200 grid for modeling. This grid is fine enough to place two points in the starting jet, but yet not overly tax the computer for storage and run time. Comparison to a 100 by 400 grid showed no change in either flowfield or free surface shape. Figure 5 shows a double grid run comparable to figure 2.

<u>On Laminarity of the Jet Inflow</u>

Classic analysis of the liquid in liquid jet indicates very low stability. Reference 35 shows a limit as low as Re = 11. Mcnaughtoun and Sinclair using a more practical analysis divided the liquid in liquid jet into four regimes
dissipated laminar (Re < 300 approx.)
Fully laminar jets (300 < Re < 1000 approx.)
semi-turbulent (1000 < Re < 3000 approx)
Fully turbulent (Re > 3000)
Their transition numbers are somewhat a function of the length of their apparatus. Dissipated jets only made it a portion of the way across the test chamber before

6

dissipating into the bulk liquid via the same breakdown reported in the previous reference. This distance increased with increasing Re number until a laminar jet spanned the length of their test chamber the fully laminar region. As the Re increased further a turbulent flow region began to emerge near the far end of the jet. The length of laminar flow would begin to decrease as the flow increased until eventually the jet would become turbulent right at the nozzle marking the transition to the final region.

Their data for the length of the laminar region was given by the correlation

$$a/d = 9.97x10^7 \, \text{Re}^{-2.46} (D/d)^{-0.48} (L/d)^{0.74} \quad (26)$$

Our runs of Re 450, 630 are in the fully laminar region. The Re 900 run should transition to turbulence at a distance of 8.3 cm and Re 1290 at 3.4 cm. Aydelott reviewing the data reports the following findings. No spreading at Re 450, for Re 630 no spreading if the liquid height over the jet was less than 2.5 cm; spreading consistent with a laminar jet thereafter. Re 900 a jet intermediate between laminar and turbulent. And for Re > 1500 a fully turbulent jet. Comparison to drop tower data

Visual Comparison

Comparison of the data to the model show similarity in jet spread and flow motion. The model even captures the vortex shedding from the tip of the geyser as the flow develops although the axisymmetric nature of the model forces more regularity in the vortex shedding than is seen in the drop tower film.

Predicted Geyser Height

Model predictions of geyser heights are shown in table 2. For comparison the measured heights of Aydelott and the previous predictions of Schrader[30] (Only available for a few runs) are shown.

Figure 6 shows the comparison between predicted geyser height and fill level for the model and the experiment. Although the model underpredicts experiment for the lower flow rates it overpredicts at the highest flow rate. The overprection is believed due to the lack of turbulence modeling. It is well known that turbulent jets spread at a much higher rate than laminar jets. This increased spread will lower the centerline velocity more quickly and increase the area of the jet at the free surface, decreasing the amount of surface deformation required to contain the jet. The under prediction is harder to explain but is worse at low fill levels. It may be due to a slosh baffle at the 33% full level which prevents development of a hemispherical

Table 2 Geyser Height Comparison

Test	Model Ratio of Geyser height to tank radius	Prediction of Schrader	Measured Ratio of Geyser height to tank radius
1	0.22	N/A	0.55
2	0.4	N/A	.80
12	0.12	N/A	.36
13	0.42	0.36	.84
14	2.7	N/A	2.16
15	0.06	N/A	.42
17	0.1	N/A	.34
19	0.28	N/A	.52
24	2.06	N/A	1.45
50	0.04	N/A	.24
51	0.1	N/A	.42
52	1.84	N/A	1.10
53	0.2	0.21	.30
57	0.84	0.45	.70
64	0	N/A	.10
65	0.16	N/A	.20
66	0.78	N/A	.48

interface in zero gravity. The baffle acts to raise the liquid height at the centerline and flatten the free surface which lessens the surface tension force on the jet. This effect was most pronounced at the 29% full runs where the measured height of the free surface above the jet is actually higher than the 39% full tests. It was felt that free suface height above the jet was the more important parameter. Therefore model runs matched the free height not the liquid fill level.

Overall agreement is reasonable. Run 14 will be difficult to match since this run is most likely unstable so the measured geyser height is limited by the tank size. Run 13 is as yet unexplained but Schrader's prediction is even more in error. For the other two runs predicted by Schrader, comparison is as follows. Run 53 both predictions are very close to each other but low. Run 57 the current prediction is much closer to the measured value.

Summary

This paper documents the adaptation of the Jacqmin algorithm to the problem of restraint of liquid jets. Adaptations include formulation of an axisymmetric fourth order model, implementation of a symmetric boundary condition at the tank centerline, and enhancement of the wall wetting boundary condition to fourth order accurate. A simple velocity forcing function has been added to simulate the jet without violating continuity. Figures demonstrate the code's

ability to model jet flows. Comparison to drop tower data shows the strength and validity of this code. Finally, the limits of surface tension in restraining liquid jets have been found and the growth rate of geysers after this limit has been exceeded calculated.

References

1. Jacqmin, D. "Calculation of Two-Phase Navier-Stokes Flows Using Phase-Field Modeling" Journal of Computational Physics 155, 96-127, 1999

2. Symons, E.P.; Nussle, R.C. and Abdalla, K.L. "Liquid Inflow to Initially Empty, Hemispherical Ended Cylinders During Weightlessness": NASA TN D 4628: June 1968

3. Symons, Eugene P., Nussle, Ralph C., "Observations of Interface Behavior During Inflow to an Elliptical Ended Cylinder in Weightlessness", NASA TM X-1719, January 1969

4. Symons, Eugene P. "Interface Stability During Liquid Inflow to Initially Empty Hemispherical Ended Cylinders in Weightlessness", NASA TM X-2003, April 1970

5. Symons, Eugene P., Staskus, John V., "Interface Stability During Liquid Inflow to Partially Full, Hemispherical Ended Cylinders in Weightlessness", NASA TM X-2348, August 1971.

6. Staskus, John V, "Liquid Inflow into a Baffled Cylindrical Tank During Weightlessness", NASA TM X-2598, August 1972.

7. Spuckler, Charles M. "Liquid Inflow to Initially Empty Cylindrical Tanks in Low Gravity", NASA TMX-2613, August 1972.

8. Labus, T.L., Aydelott, J.C., Andracchio, C.R., "Effect of Baffles on Inflow Patterns in Spherical Containers During Weightlessness", NASA TMX-2670, November 1972.

9. Symons, Eugene P., "Effect of Throttling on Interface Behavior and Liquid Residuals in Weightlessness", NASA TM X-3034, May 1974

10. Aydelott, J.C. "Axial Jet Mixing of Ethanol in Spherical Containers During Weightlessness": NASA TM X-3380: April 1976

11. Labus, Thomas L., "Liquid Jet Impingement Normal to a Disk in Zero Gravity", NASA TP 1017, August 1977.

12. Aydelott, J.C. "Axial Jet Mixing of Ethanol in Cylindrical Containers During Weightlessness"; NASA TP-1487: July 1979

13. Aydelott, J.C.: "Modeling of Space Vehicle Propellant Mixing" NASA TP-2107: January 1983

14. Bentz, M.D., et al. "Tank Pressure Control Experiment - A Low-g Mixing Investigation," AIAA 90-2376

15. Bentz, Michael D., "Tank pressure control in low gravity by jet mixing", NASA-CR-191012, March 1993

16. Bentz, M. D; Knoll, R. H; Hasan, M. M; Lin, C. S.; "Low-g fluid mixing - Further results from the Tank Pressure Control Experiment" AIAA PAPER 93-2423, Jun. 1993

17. Hasan, Mohammad M., Lin, Chin S., Knoll, Richard H., and Bentz, Michael D., "Tank Pressure Control Experiment: Thermal Phenomena", NASA TP 3564, March 1996.

18. Bentz, Michael D, et. al. "Tank Pressure Control Experiment - Results of three space flights", AIAA Paper 97-2816, July 1997

19. Chato, D. J; and Martin, T. A.; "Vented Tank Resupply Experiment - Flight Test Results," AIAA 97-2815, July 1997.

20. Concus, P., "Capillary Stability in an Inverted Rectangular Tank", Adv. Astro. Sc. Vol. 14, pp. 21-37, 1963

21. Concus, P., "Static Menisci in a Vertical Right Circular Cylinder," J. Fluid Mech. Vol 34, part 3 pp. 481-495, 1968

22. Nickell, R. E., Tanner, R. I., Caswell, B. "The solution of viscous incompressible jet and free surface flows using finite element methods" J. Fluid Mechanics vol. 65, part 1, pp. 189-206, 1974

23. Hochstein, J.I., Gerhart, P.M., Aydelott, J.C., Computational Modeling of Jet Induced Mixing of Cryogenic Propellants in Low-G, AIAA 84-1344

24. Hochstein, J. I. "Computational Modeling of Jet Induced Mixing in Cryogenic Propellant Tanks in Low-G", Ph.D. Thesis, The University of Akron, 1984.

25. Aydelott, J.C., et al., "Numerical Modeling of On-Orbit Propellant Motion Resulting from an Impulsive Acceleration," NASA TM-89873, 1987

26. Der, J.J., Stevens, C.L., Low-Gravity Bubble Reorientation in Liquid Propellant Tanks, AIAA 87-0622, January 1987.

27. Tegart, James, "Three-Dimensional Fluid Interfaces in Cylindrical Containers" AIAA 91-2174, June 1991.

28. Brakke, K. A. "Surface Evolver Manual" Minimal Surface Team of the Geometry Supercomputer, Available via ftp at geom.umn.edu

29. Brackbill, J.U., Kothe, D.B., Zemach, C., "A Continuum Method for Modeling Surface Tension," *Journal of Computational Physics v100 n2*, June 1992.

30. Schrader, G. B, and Hochstein, J. I., "Modeling of Jet-Induced Geyser Formation in Low-Gravity," AIAA 93-0256, January 1993.

31. Van der Waals, J. D.,*The Thermodynamic Theory of Capillarity Flow Under the Hypothesis of a Continous Variation of Density* (Verhandel/Konink. Akad. Weten., 1893), Vol 1; English Translation, *Journal of Statistical Physics* Vol. 20.

32. Cahn, J. W., and Hillard, J. E., "Free Enegy of Nonuniform Systems. III. Nucleation in a Two-Component Incompressible Fluid," *Journal of Chemical Physics V31 n3,* September 1959.

33. Collatz, L. *The Numerical Treatment of Differential Equations* (3ed.), Springer-Verlag, Berlin 1966.

34. Viilu, A., "An Experimental Determination of Minimum Reynolds Number for Instabiltiy in a Free Jet," *Journal of Applied Mechanics,* ASME September, 1962.

35. McNaughton, K. J., and Sinclair, C. G., "Sumerged Jets in Short Cylindrical Flow Vessels," *Journal of Fluid Mechanics,* Vol 25., ASME 1966.
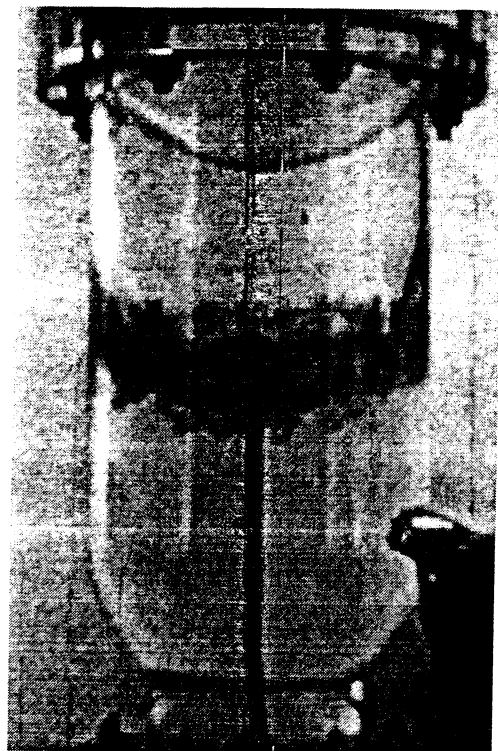
a) Start

b)   0.93 seconds
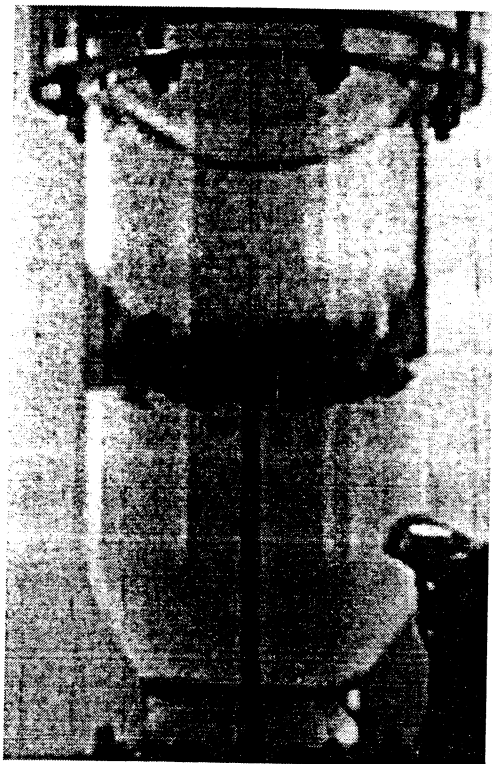
c) 2.04 seconds

d) 3.10 seconds
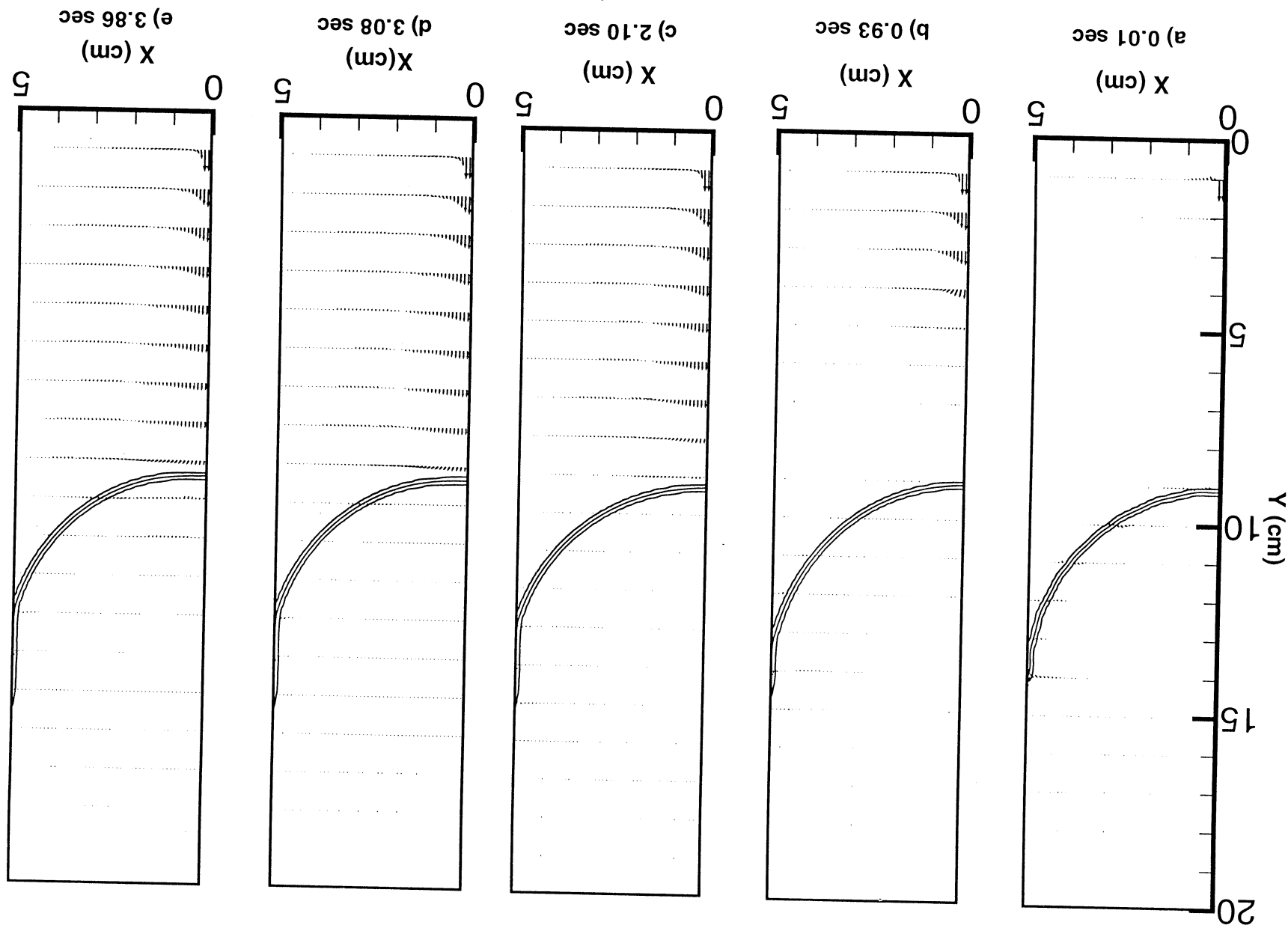
Figure 1 Drop Tower Run 15 Fill 50% Jet Velocity 17 cm/s

Figure 2 Time sequence of free surface and velocities Fill 50% Jet velocity 17 cm/s
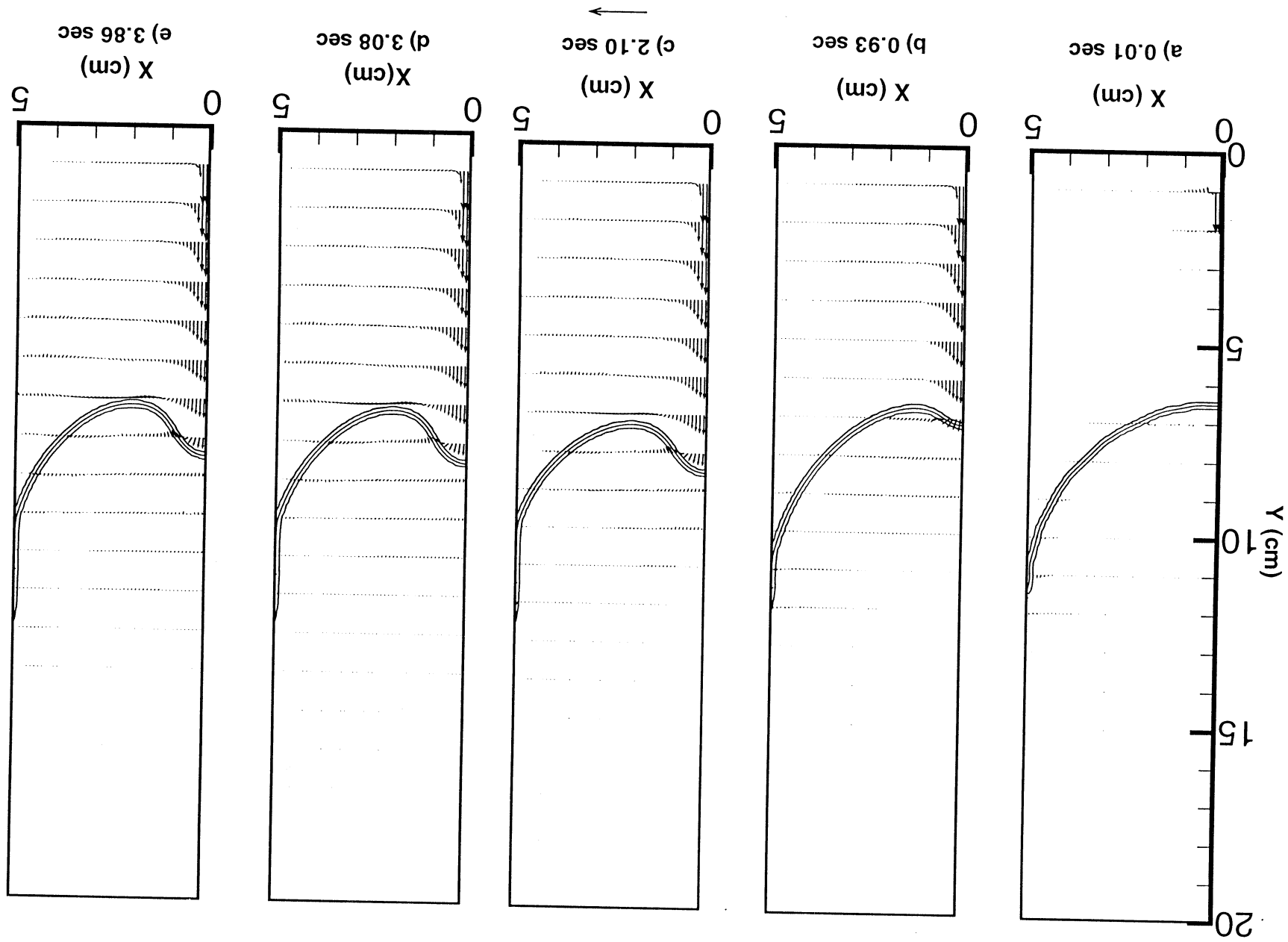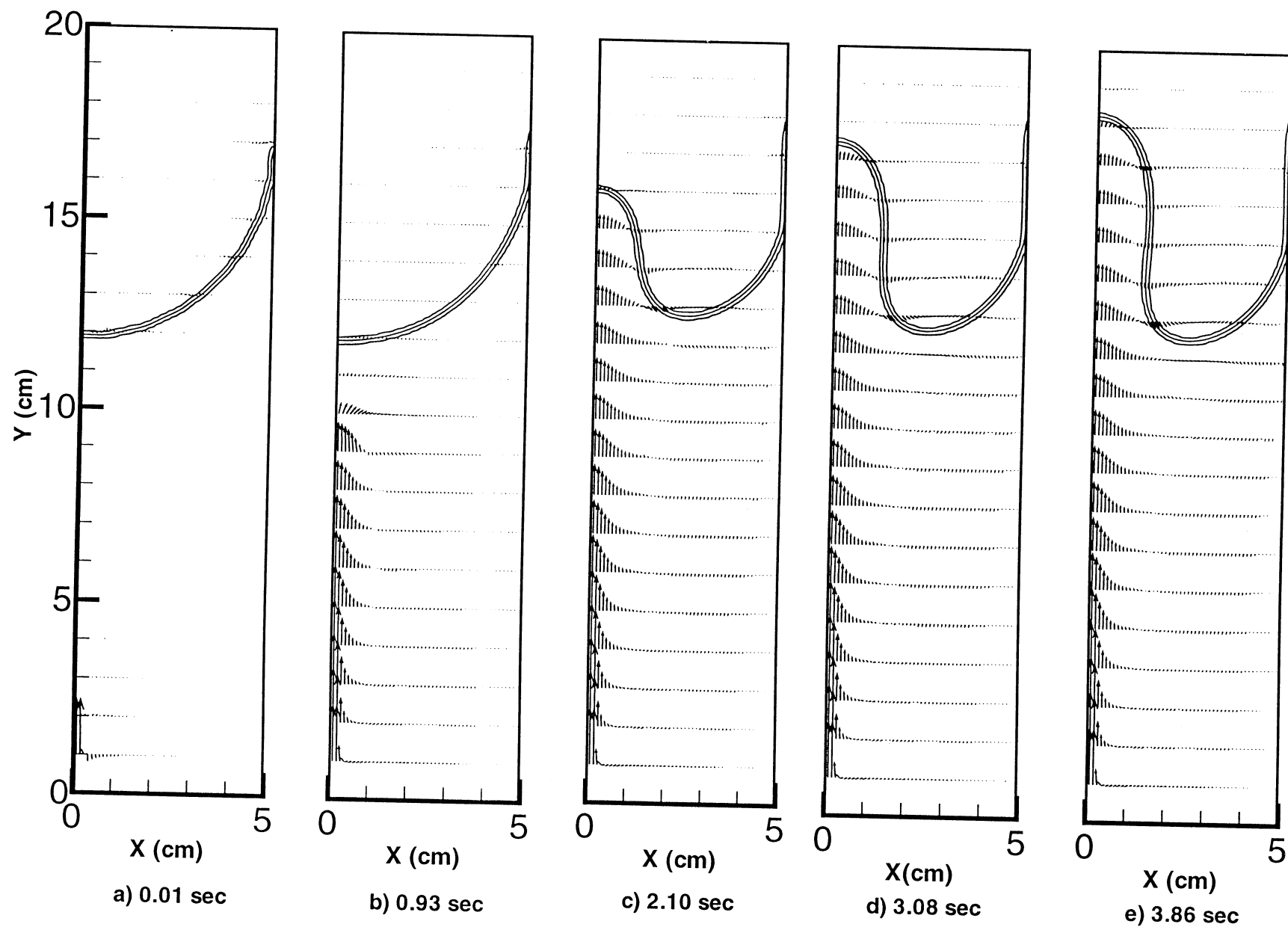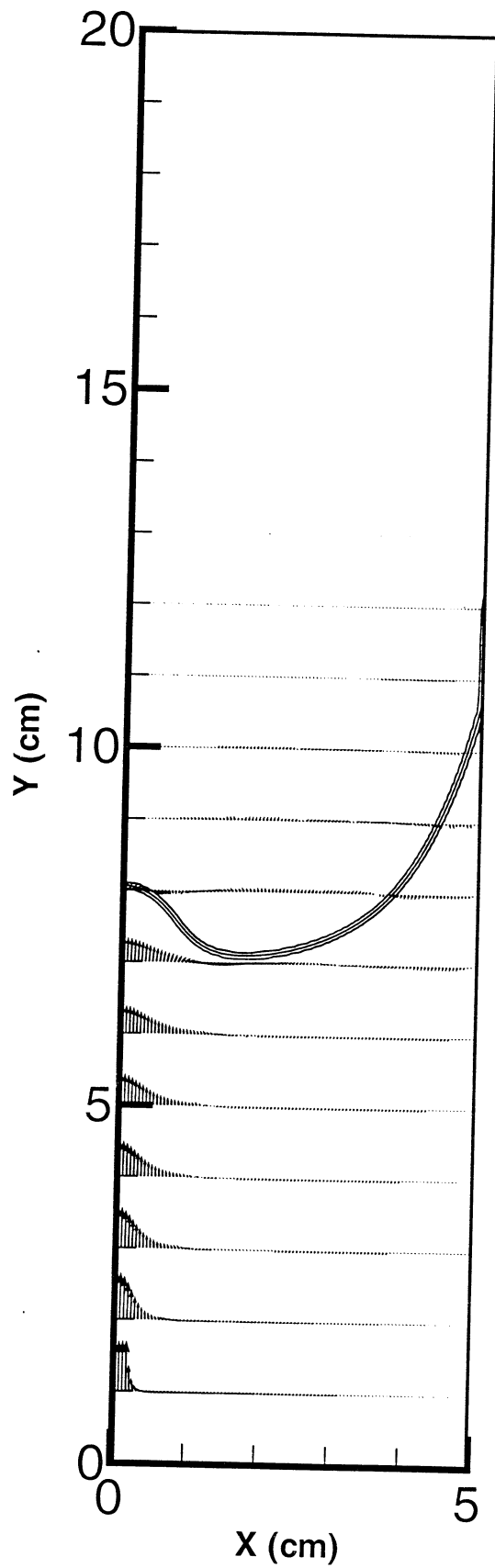
Reference Vector 50 cm/s

a) 0.01 sec
X (cm)

b) 0.93 sec
X (cm)

c) 2.10 sec
X (cm)

d) 3.08 sec
X (cm)

e) 3.86 sec
X (cm)

Y (cm)

Figure 3 Time sequence of free surface and velocities Fill 39% Jet velocity 34 cm/s

Reference Vector 50 cm/s

a) 0.01 sec
X (cm)

b) 0.93 sec
X (cm)

c) 2.10 sec
X (cm)

d) 3.08 sec
X(cm)

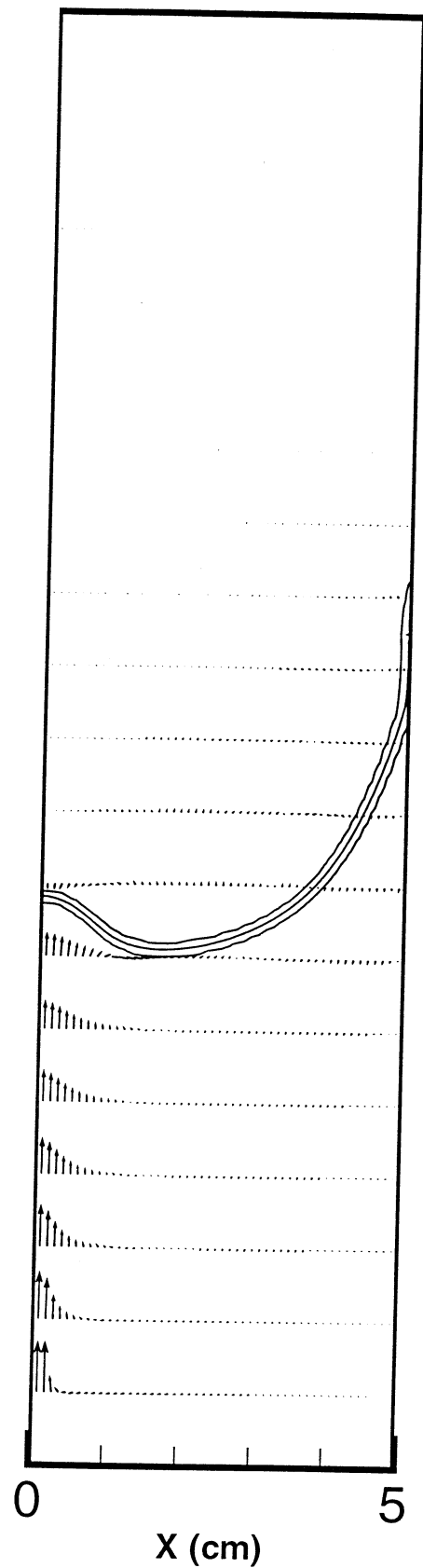e) 3.86 sec
X (cm)

Y (cm)

Reference Vector 50 cm/s

Figure 4 Time sequence of free surface and velocities Fill 73% Jet velocity 48 cm/s

a) Double Grid 0.92 sec

b) Single Grid 0.93 sec

Reference Vector 50 cm/s

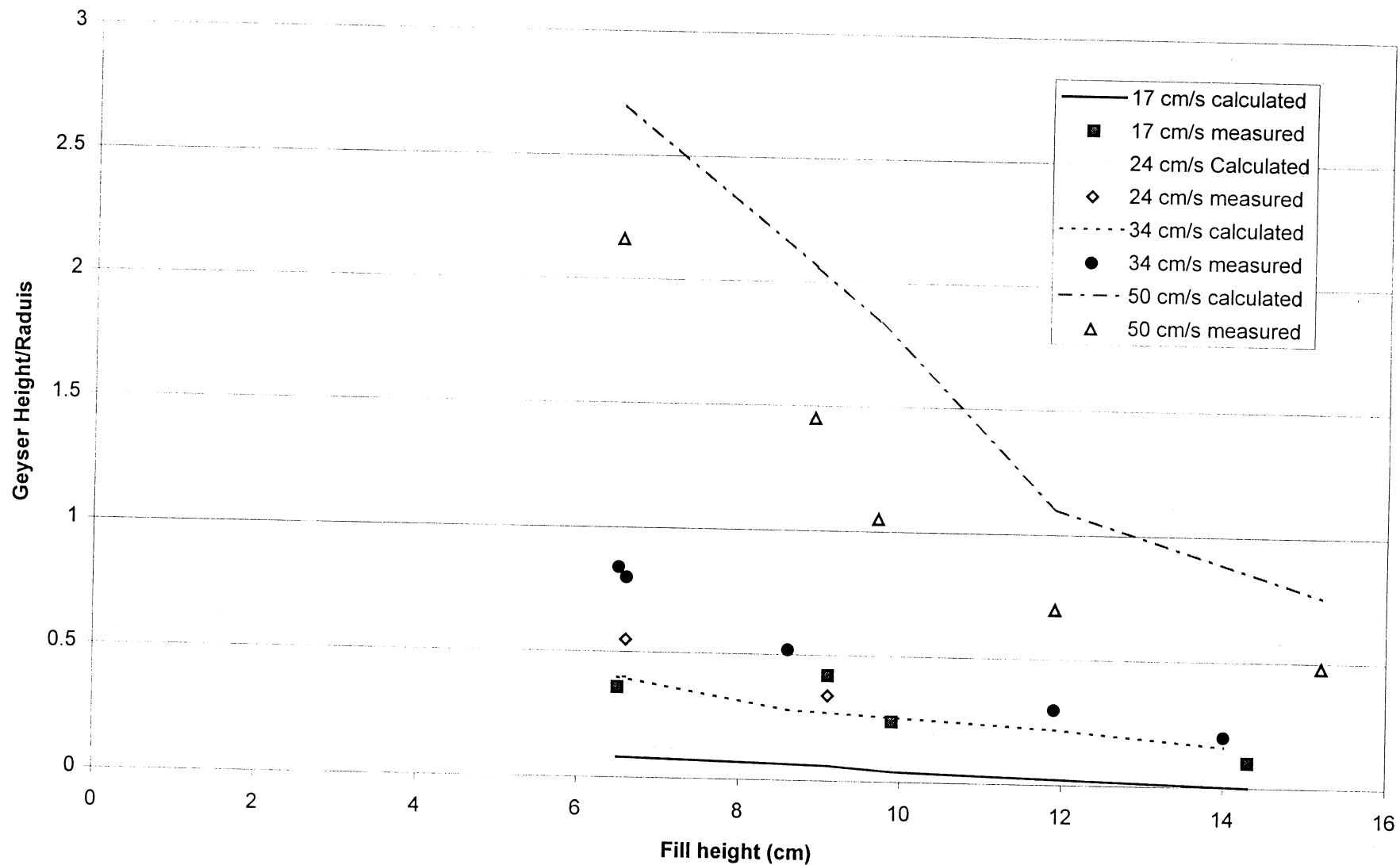Figure 5 Comparision between single and double grid solution Fill 39% Jet velocity 34 cm/s

Figure 6 Non-Dimensional Geyser Height Comparision Caculated vs Measured